Journal of the mechanical behavior of biomedical materials 66 (2017) 68–76

Contents lists available at ScienceDirect

Journal of the Mechanical Behavior of Biomedical Materials

journal homepage: www.elsevier.com/locate/jmbbm

Strain rate dependency of fractures of immature bone

Vee San Cheong[a], Angelo Karunaratne[a], Andrew A. Amis[b,c], Anthony M.J. Bull[a,*]

[a] Department of Bioengineering, Imperial College London, London SW7 2AZ, United Kingdom
[b] Mechanical Engineering Department, Imperial College London, London SW7 2AZ, United Kingdom
[c] Musculoskeletal Surgery Group, Department of Surgery & Cancer, Imperial College London School of Medicine, London W8 6RF, United Kingdom

ARTICLE INFO

Keywords:
Structural stiffness
In-vitro biomechanical testing
Oblique fracture
Child abuse
Non-accidental injury
NAI

ABSTRACT

Radiological features alone do not allow the discrimination between accidental paediatric long bone fractures or those sustained by child abuse. Therefore, there is a clinical need to elucidate the mechanisms behind each fracture to provide a forensic biomechanical tool for the vulnerable child. Four-point bending and torsional loading tests were conducted at more than one strain rate for the first time on immature bone, using a specimen-specific alignment system, to characterise structural behaviour at para-physiological strain rates. The bones behaved linearly to the point of fracture in all cases and transverse, oblique, and spiral fracture patterns were consistently reproduced. The results showed that there was a significant difference in bending stiffness between transverse and oblique fractures in four-point bending. For torsional loading, spiral fractures were produced in all cases with a significant difference in the energy and obliquity to fracture. Multiple or comminuted fractures were seen only in bones that failed at a higher stress or torque for both loading types. This demonstrates the differentiation of fracture patterns at different strain rates for the first time for immature bones, which may be used to match the case history given of a child and the fracture produced.

1. Introduction

For immature human bones, it is not possible to differentiate between fractures sustained from child abuse and those caused accidentally solely from radiological features (Leventhal, 1999), even though various injury mechanisms have been proposed (Haney et al., 2009; Pierce et al., 2004). Therefore, there is a clear need to understand paediatric whole bone failure mechanisms (Ebacher et al., 2007; Kress et al., 1995; Ouyang et al., 2003).

Among the many fracture patterns seen clinically, spiral, oblique and transverse long bone fractures are the most common, making it difficult to diagnose non-accidental injury (NAI) in such cases (Caffey, 1946; Carty, 1993). The prospect of using engineering tools to interpret the verbal description of an injury mechanism from either the child or the carer, would allow a level of confidence to be assigned to the described injury mechanism responsible for the observed fracture. It is, therefore, important to be able to link the loading mechanism to the fracture type. In order to achieve this, an experimental method needs to be developed to create a consistent reproduction of relevant fractures. This would then allow their replication in a computer model that could be used as an objective tool to assist in the detection of NAI. This would be especially necessary to prevent situations where NAI is missed, as the child may suffer from further physical and emotional abuse, thereby stunting his/her eventual growth and intellectual and emotional development, or even resulting in death (Jayakumar et al., 2010; Stotts, 2007). Conversely, a wrongful accusation of innocent families may lead to the unwarranted separation of the family and child (Kowal-Vern et al., 1992; Pierce and Bertocci, 2008).

There are only three studies that have investigated the fracture tolerance of the immature population using whole bones, namely that by Forman et al. (2012) and Ouyang et al. (2003) for humans, and Pierce et al. (2000) for pigs. However, the latter is the only work in the literature that had the intended aim of reproducing fractures seen in child abuse (Pierce et al., 2000). Porcine femora were used in their study, where the age equivalence of the specimens assumed that one week in pigs is approximately equivalent to a year in humans (Baumer et al., 2009). Their experiments were conducted at rates of 1 mm/s for three-point bending and 1 $°s^{-1}$ for torsional loading. These fall under the quasi-static strain rate regime (Cristofolini et al., 2010), which is too low to reproduce injuries caused during child abuse, as they usually happen at higher loading rates (Miltner and Kallieris, 1989).

Three-point bending has been the test of choice, because it is able to model the event when a bone is impacted by an object (Pierce et al., 2000); this is a known mechanism of injury in child abuse (Hobbs, 1989). Yet, unlike the consistent transverse fractures reported by Pierce et al. (2000) in all 12 immature porcine femora at low strain

* Corresponding author.
E-mail address: a.bull@imperial.ac.uk (A.M.J. Bull).

http://dx.doi.org/10.1016/j.jmbbm.2016.10.023
Received 5 May 2016; Received in revised form 3 October 2016; Accepted 16 October 2016
Available online 02 November 2016

rate, Forman et al. (2012) reported that fractures in the immature population were rarely initiated at the mid-diaphysis at high strain rates. Instead, oblique or comminuted fractures ensued from cracks that were initiated off-centre. The presence of multiple types of fracture patterns is consistent with the study conducted by Kress et al. (1995), who impacted 253 tibiae and 136 femurs from the geriatric population at a high velocity of 1.2–7.5 ms^{-1} and found comminuted butterfly fractures and oblique fractures to be the most common. Unfortunately, no fracture patterns were available from the study by Ouyang and colleagues (2003) at both low and high strain rates as the tests were terminated when the slope of the force-time curve dropped to zero. Therefore, the generation of a consistent fracture pattern at high strain rate has not been confirmed.

The three-point bending test poses problems, because the curvature and variation in cross-section of long bones along their length may cause high shear stress at the mid-length of the specimen during testing, where it is most likely to fail. The complex geometry of bone also increases the possibility of the specimen failing in shear rather than in tension, which makes the analysis of the failure more difficult. Moreover, it has been recommended that the specimens used in three-point bending tests should be straight and have a uniform cross-section (Athanasiou et al., 2000). Thus, four-point bending tests are more suited to study the case of bending as the middle section of the bone would experience a constant bending moment, thus resulting in pure direct stress for a bone of constant, symmetrical, cross section, but these tests have not been conducted on immature bone.

Spiral fractures have been consistently produced in all the works involving torsion of intact whole mature bones. Torsional loading of sheep femora produced spiral fractures in the mid-diaphysis consistently in the work of Wullschleger (2010). A combination of longitudinal and spiral fractures was reported by Taylor et al. (2003), who tested mature chicken metatarsals to failure using torsional cyclic testing at 3 Hz. It is therefore interesting to note that testing of immature porcine femur at a rate of 1 $°s^{-1}$ failed to generate a spiral fracture consistently (Pierce et al., 2000). Despite attempts made to reduce the working length of the specimens, growth plate separation continued to be the dominant failure mode. Spiral fractures have also been produced in the three-point bending work of Kress and co-workers (1995), who noted the correlation with the presence of a torsional load, yet perhaps this is also due to the presence of shear stress in combination with direct stress, producing a principal direct stress oblique to the bone long axis. However, the failure to generate consistent spiral fractures in immature bone further compounds the problem by questioning when spiral fractures, which are seen commonly among children (Hobbs, 1989), are produced.

The aims and objectives of this paper were to design an experimental apparatus to enable testing of immature long bones in bending and torsion, characterise the mechanical behaviour of immature bone to the point of failure at multiple strain rates, and to investigate if consistent fracture patterns are produced in bending and torsion across strain rates.

2. Materials and methods

Twenty ovine tibiae from 5 months old British Texel lambs were harvested after slaughter. A month in sheep corresponds to a year in human (Nafei et al., 2000). Ovine tibia has a similar aspect ratio to human tibia and the former can be considered similar to the latter but scaled down by a third (Finlay et al., 1995; Osterhoff et al., 2011). Four bones were used for each set of experiments: two torsional loading experiments and three four-point bending tests. The bones were cleaned of all soft tissues, leaving the periosteum intact as far as possible, before they were wrapped in cloth soaked in 1% Phosphate Buffered Solution (PBS). The bones were then double bagged and frozen at -20 °C for storage, as the strength of the bone has been found to remain unchanged by the process of freezing (Moreno and Forriol, 2002). The bones were stored for a maximum of one year and they were defrosted in a cool box in their sealed bags 6 h prior to the start of mechanical testing. The bones were kept hydrated by misting them with water every 5 min. Strain gauges were affixed for a computational study; these results are not presented here.

2.1. Image acquisition and specimen alignment

Thawed bones underwent micro-CT scanning with the tissue paper intact in a Metris X-Tek HMX ST 225 CT System (Nikon Metrology, Tring, UK). A 1 mm copper filter was used as the reflection target, with a focal spot size of 5 μm and the X-rays were set at 200 kV and 200 μA. A resolution of 115 μm was achieved. The 3D reconstructions of the scans were used to generate solid models for geometrical analysis to align the specimens.

The landmarks used to align the bone in four-point bending and torsion were calculated from a specimen-specific alignment system (Cheong and Bull, 2015). In brief, this methodology optimised bones to experience *near* pure shear, and *near* pure direct stress in torsion and bending, respectively. This was achieved via the solid mechanics principles that: for any object, there exists a set of principal axes where the structure would experience maximum and minimum stresses; pure torsion produces pure shear in a perfectly symmetrical structure; and four point bending produces a pure bending moment with no shear stresses within the inner span in a symmetrical structure. The results of the geometrical analysis were used to determine the distances between the rollers in four-point bending, and the level of fixation of bones for torsion. In all cases the 4:1 width-to-span ratio for simple bending and torsion, as found by Hardy and Pipelzadeh (1991), who found that this was the minimum required to prevent deep flexion, was maintained.

2.2. Mechanical testing

The tests were conducted on an Instron 8874 universal materials testing machine (Instron – Division of ITW Limited, High Wycombe, UK), using linear displacement or angular control. The synchronous recording of forces, torques, translations and rotations was achieved via a custom-written LabVIEW program, which also controlled the actuator of the Instron machine and obtained data at 0.2 ms intervals. The process of fracture propagation was captured by a high-speed video camera (Phantom v126, Vision Research, Wayne, NJ, US). A frame rate of 7000–10000 fps was used depending on the actual frame of view and lighting conditions. The fracture morphology was classified based on the crack initiation observed in the high-speed videos.

To characterise the structural behaviour of ovine tibiae, four-point bending tests to failure were conducted at three different loading rates: 50 mm/s ($\dot{\varepsilon}$: 0.1–0.3 s^{-1}), 25 mm/s ($\dot{\varepsilon}$: 0.08–0.1 s^{-1}), and 1 mm/s ($\dot{\varepsilon}$: 0.003–0.004 s^{-1}), using the specimen-specific alignment system. All the bones were tested in the sagittal plane, with the posterior side of the bone in tension, using a custom-made jig to minimise the transmission of unintended forces and torques (Fig. 1). Two rounds of preconditioning were conducted before testing the bone to failure. Each specimen was preconditioned by loading at a constant velocity of 0.5 mm/s until the crosshead moved 1.5 mm. The bone was then unloaded at a speed of 0.01 mm/s, followed by an interval of 5 min before the next run took place. For failure testing, loading was halted when a displacement of 4 mm was reached (5 mm for the slowest tests), which was determined from a pilot test to be the limit to cause fractures.

For torsional loading, 16 right tibiae were used with the proximal part externally rotated relative to the distal part. The bones were potted in stainless steel pots using Polymethyl Methacrylate (PMMA) bone cement (Simplex Rapid, Austenal Dental Products Ltd, UK). The distal pot was then attached to a rocker base, which had ball bearings attached to it to allow it to slide on an XY table, which eliminated the transmission of unintended forces to the bone (Fig. 1); the absence of a

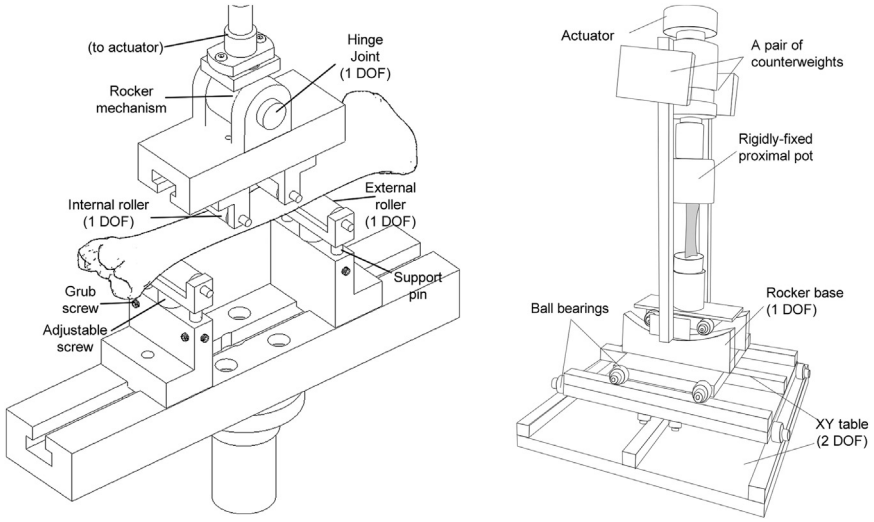

Fig. 1. (Left) Experimental setup for four-point bending. The rocker mechanism that is attached to the actuator (not shown) ensures contact is always maintained with the bone. The external rollers are adjustable in height to allow alignment of the bone along its principal direction. (Right) The experimental setup for torsional loading. The proximal pot is rigidly affixed to the actuator, while the distal pot is connected to a rocker, which can slide on the XY table. Mirrors were used to capture the full view around the bone. DOF stands for degree of freedom.

rocker base would result in loading being applied at an offset from the neutral axis due to the bone not being perfectly cylindrical. This would then introduce unwanted shear stress caused by bending. Preconditioning tests were carried out. An actuator speed of 5.6 °s^{-1} was applied until a rotation of 5° was reached. The bone was then unloaded at a rate of 0.05 °s^{-1}. To relieve any residual stress, the distal pot was disconnected from the XY table for a minimum of 5 minutes. Testing then took place at either 196 °s^{-1} ($\dot{\varepsilon}$: 0.07–0.2 s^{-1}) or 19.6 °s^{-1} ($\dot{\varepsilon}$: 0.006–0.02 s^{-1}) until an angle of 39.2° was reached.

2.3. Statistical analysis

The force-displacement and torque-angle graphs obtained showed a high degree of linearity. To detect the onset of plastic deformation, linear regression and the associated coefficient of determination (R^2) was also computed for 0–80%, 0–90%, 0–99% and 0–100% of each of the curves, using a method first detailed in Juszczyk et al. (2011).

The bending stiffness was calculated from the force-displacement curve for up to 90% of the fracture load as the R^2 showed a high linearity of 0.99 for each case with the exception of one test (0.98). Data below 0.5 kN were not used in the calculation as all the curves exhibited a toe-region at the initial region due to the internal rollers coming into full contact with the bone. The energy to failure was calculated by integrating the area under the force-displacement curve for each bone, using the trapezoidal rule function in the statistical software. One-way analysis of variance across the three strain rates was conducted using the non-parametric Kruskal-Wallis test, as normality could not be assumed due to the small number of specimens used for each test, followed by Mann-Whitney U test to identify regions of significant difference. The bending stiffness was subsequently re-grouped according to the fracture patterns obtained to check for differences using the Mann-Whitney U test, where a p-value below 0.05 was taken to be significant. The same procedure of analysis was applied to the results of the torsional tests, where the toe region of 5Nm was ignored. All statistical analyses were conducted using OriginPro 9.0 (OriginLab Corp., Northampton, MA).

3. Results

3.1. Four-point bending

Bone fracture took place in 64.3 ± 8.6, 79.9 ± 19.7 and 1402.8 ± 144.9 ms at fast, medium and slow tests, respectively. All fractures were characterised by a sudden drop in force. Every measured force-displacement curve had almost the same curvilinear pattern, with a toe-region where the internal rollers of the four-point bending fixture came into full contact with the bone, followed by a highly linear region. The curves displayed varying amounts of plastic deformation prior to failure at each strain rate (Fig. 2 - left). The coefficients of determination calculated for increasing portions of the force-displacement curves showed that the curves were highly linear up to 99% of the fracture force, with a minimum R^2 value of 0.98 for all three groups.

The energy absorbed to failure suggested a larger range in the fast and medium groups at 5.60–12.66 J and 1.86–9.50 J, respectively, compared to that from the slow group at 7.22–9.08 J, but the population variance was not significant (p = 0.171, Levene's test) (Table 1). There was also no statistically significant difference in energy absorbed (p = 0.246).

Fig. 3 contains video frames showing how the crack propagated in transverse and oblique fracture patterns. In the slow group, all the bones broke within the region of constant bending moment, resulting in a transverse fracture pattern (Fig. 3 - top). Incomplete greenstick fractures were obtained for two cases. In both the medium and fast groups, there were two bones in each group that failed within the region of constant bending moment and two whose fractures initiated at the region between the internal and external supports. The resulting fracture pattern was thus oblique and, in all four cases, the crack initiated at the proximal part of the bone (Fig. 4). In one case where the initial fracture was transverse, an oblique fracture developed later, resulting in a butterfly wedge fracture. This case was accompanied by more plastic deformation than for the other bones. When examined under a microscope, bones that were tested at slow strain rate exhibited a rough surface with evidence of fibre pull-out whereas the fracture surfaces of the bone that fractured obliquely were smooth (Fig. 5).

The tibiae had bending stiffnesses of 1.94 ± 0.29, 2.12 ± 0.39 and 1.36 ± 0.15 kN/mm (mean ± SD) from the fast, medium and slow groups respectively (Table 1). The bending stiffness of the tibiae in the fast and medium groups were both significantly greater than that from the slow group (p = 0.014 for both) (Table 1). When the results from the medium and fast groups were regrouped based on their fracture patterns, the mean bending stiffness of tibiae that had an oblique fracture pattern was 24.9% higher than those with transverse fracture patterns (p = 0.014). However, the peak and fracture forces were not significantly different.

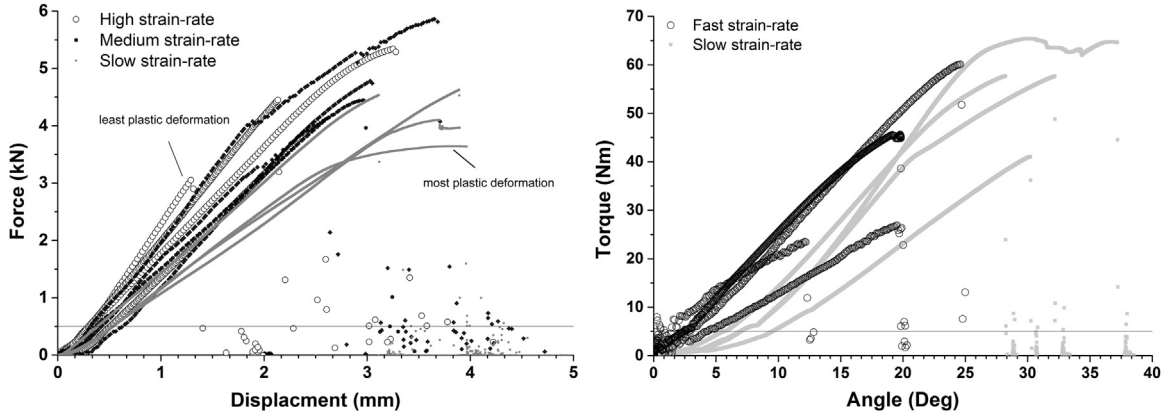

Fig. 2. (Left) Force-displacement for all the tibiae in four point bending. (Right) Torque-angle curves for all the tibiae in torsion testing. The part of the curve below the horizontal line was not included in the linear regression analysis. The two labelled curves showed the specimens that experienced the least and the greatest plastic deformation prior to failure in four point bending.

3.2. Torsional loading

A toe-region was present in all the torque-angle curves (Fig. 2 - right). The corresponding strain-torque curves show good linearity, which indicates the minimal contribution of eccentric loading. Linear regression calculated for increasing portions of the torque-angle curves showed that the curves were highly linear up to 99% of the fracture force, with a minimum R^2 value of 0.98 for all groups.

The torsional stiffness and work to fracture of the tibiae from the two groups are shown in Table 2. The mean torsional stiffnesses of the tibiae from the fast and slow groups were 2.10 ± 0.66 N m^{o-1} and 2.54 ± 0.65 Nm^{o-1}, respectively ($p = 0.243$). The corresponding energies to fracture were 416.3 ± 251.0 J and 860.0 ± 347.0 J. ($p = 0.029$) (Table 2).

The peak and fracture torque were almost coincident in all cases. The peak torque ranged from 23.5–65.4 Nm, whereas the fracture torque (the last recorded value prior to a sudden drop in torque) was between 23.4–64.6 Nm. Spiral fractures were produced in all cases. The angle of fracture was about $34.5 \pm 8.8°$ and $41.5 \pm 2.0°$ from the longitudinal axis, at lower and higher strain rates respectively, which tends towards significance ($p = 0.057$). Two different types of spiral fracture were produced (Fig. 6).

In the two cases with the highest fracture torque, multiple tiny fragments were also present together with the spiral fractures. A 'clean' spiral fracture was seen in one case but a longitudinal fracture was also present in the remaining case (Fig. 7). Only spiral fractures were seen in the remaining bones, as summarised in Table 2.

Table 1
Four-point bending test results.

Specimen	Peak force (kN)	Fracture force (kN)	Bending stiffness (kN/mm)	Energy to fracture (J)	Fracture pattern	Fracture location
BF1	4.44	4.44	1.62	6.86	Transverse	Middle
BF2	5.86	5.81	2.33	12.66	Oblique	Proximal
BF3	4.14	4.14	1.85	5.60	Oblique	Proximal
BF4	4.78	4.74	1.95	6.89	Transverse – multiple	Middle
Mean (SD)	4.81 (0.75)	4.79 (0.73)	1.94 (0.29) *	8.00 (3.16)	–	–
BM1	3.05	2.90	2.65	1.86	Oblique	Proximal
BM2	5.34	5.29	1.85	9.50	Transverse – butterfy	Middle
BM3	4.07	4.07	1.80	4.62	Transverse	Middle
BM4	4.45	4.45	2.18	4.64	Oblique	Proximal
Mean (SD)	4.23 (0.95)	4.18 (0.99)	2.12 (0.39) +	5.16 (3.18)	–	–
BS1	4.63	4.63	1.24	9.08	Transverse	Middle
BS2	4.54	4.54	1.57	7.22	Transverse	Middle
BS3	4.10	3.96	1.27	8.58	Transverse	Middle
BS4	3.64	3.64	1.36	8.91	Transverse	Middle
Mean (SD)	4.23 (0.45)	4.19 (0.47)	1.36 (0.15) *+	8.45 (0.85)	–	–

There was a significant difference between the bending stiffness of the bones tested at low strain rate and the ones from a higher strain rate, which are indicated by * and +. BF, BM and BS stand for bones from the fast, medium and slow groups, respectively.

4. Discussion

This study developed and utilized a custom-designed experimental setup to conduct four-point bending and torsional loading tests on immature ovine tibiae using a specimen-specific alignment system. No previous study has conducted four-point bending of immature bone to failure. Transverse fracture patterns were consistently produced at low strain rates of 0.003–0.004 s^{-1} while only half of the specimens exhibited transverse fractures at higher strain rates of 0.08–0.3 s^{-1}, demonstrating a strain-rate dependent effect. High-speed video recordings of the experiment documented the entire fracture process from crack initiation to failure and showed that all crack initiation took place in less than 0.1 ms. Transverse fractures initiated in the region of constant bending moment whereas oblique fractures were found to initiate proximally, in between the internal and external rollers at the region of high shear stress. Linear regression conducted on increasing portions of the force-displacement curve revealed that the immature ovine tibiae behaved linearly up to 99% of the fracture force. The bending stiffness of whole immature tibiae in the medium and fast groups (strain rates of 0.08–0.3 s^{-1}) was also characterised and classified based on the fracture patterns. It was found that bones that had oblique fracture patterns had significantly higher bending stiffness than bones that failed transversely even though the fracture force was similar.

The primary aim of this study was to test the hypothesis that reproducible fracture patterns in pure bending and torsion at different strain rates can be produced by using a specimen-specific alignment system based on its principal directions. The consistent production of spiral fractures across strain rates, and the generation of transverse fracture pattern in four-point bending at slow strain rate support the hypothesis.

4.1. Torsional loading tests

No prior work had managed to generate spiral fractures so consistently in immature bones (Wullschleger, 2010). Pierce et al. (2000) attempted to produce spiral fracture in immature porcine femora in-vitro without notching their specimens, but they obtained

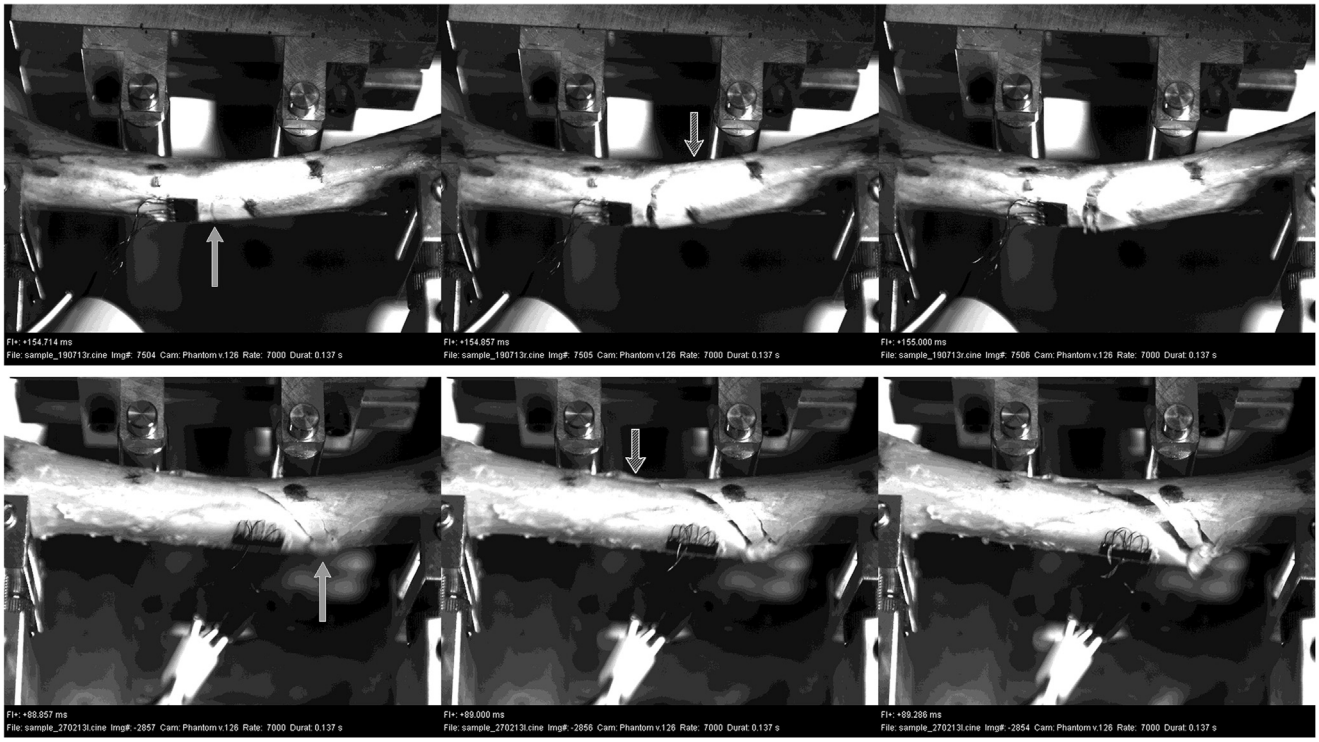

Fig. 3. (Top) The progression of a transverse fracture that took place over 0.286 s in three video frames for a tibia tested at the low strain rate (specimen BS1). (Bottom) The progression of an oblique fracture is shown here over a total of 0.429 ms tested at the medium strain rate (specimen BM4). The light grey arrows point to the location of crack initiation. Both cases show a longitudinal crack path that developed on the compressive side of the bone (patterned arrow).The acquisition frame rate in both cases was 7000 fps.

mainly fractures at the epiphyseal plates. They reported a fracture torque of 1.4–3.6 Nm, which is an order of magnitude lower than the results presented here.

Torsional tests to failure of mature human tibiae had a maximum torque of about 50Nm when tested at a rate of 1 $°s^{-1}$ (Varghese et al., 2011). In mature Merino Wethers sheep of 7–8 years old, femurs loaded in angular control at a constant velocity of 600 $°s^{-1}$ had a maximum torque of 62.7–63.1 Nm and a torsional stiffness of 0.51–0.65 Nm^{o-1} (Wullschleger, 2010). The mean torque of 55.2 Nm from the slow group of this study was slightly lower than the ultimate torque obtained for mature ovine femurs, whereas the mean torsional stiffness of 2.54 Nm^{o-1} was much higher, but it is important to note that all the above-mentioned setups did not have a mechanism to eliminate the transmission of unintended forces. However, the torsional stiffness found in this study was similar to the values of 2.6 Nm^{o-1}, obtained when human tibiae were loaded at 0.2 $°s^{-1}$, using a similar setup to that in this study (Cristofolini and Viceconti, 2000).

Spiral fractures were consistently generated across strain rates, but secondary longitudinal fracture patterns occurred at the lower strain rate while comminuted fractures occurred at the higher strain rates. Moreover, tibiae loaded at strain rates higher than 0.07 s^{-1} behaved linearly up to failure, but tibiae from the slower group experienced higher plastic deformation prior to failure and higher energy to fracture. Spiral fractures were consistently generated across strain rates of 0.006–0.2 s^{-1}, which suggests that the secondary fractures were the result of strain-dependency effects.

From an analytical perspective, the application of a torque causes shear stress and strain to be developed on both the transverse (cross-section) and axial planes, the latter due to the complementary effect of shear (Fig. 8A). As bone is a transversely isotropic material, its shear

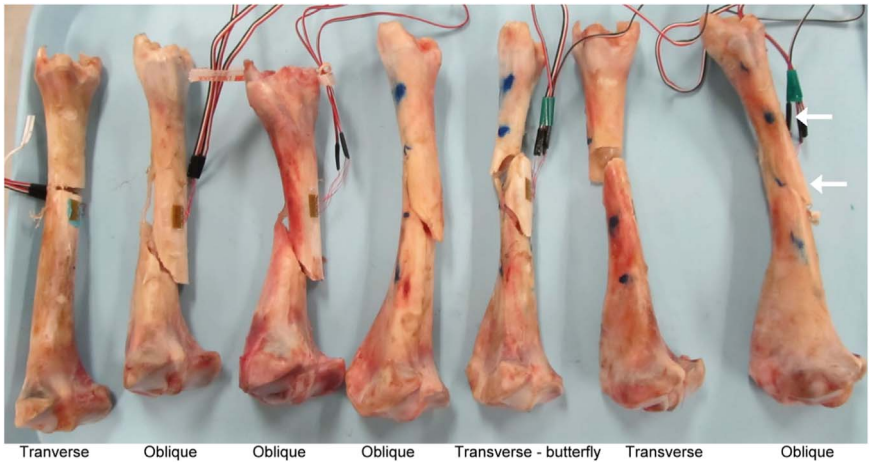

Fig. 4. Fractured bones from the fast (first three) and the medium groups. The middle two dots in each bone, as indicated by the arrows, marked the region of constant bending moment in four-point bending. All oblique fractures occurred proximally. A transverse fracture that later progressed into a butterfly fracture can be seen in the third bone from the right.

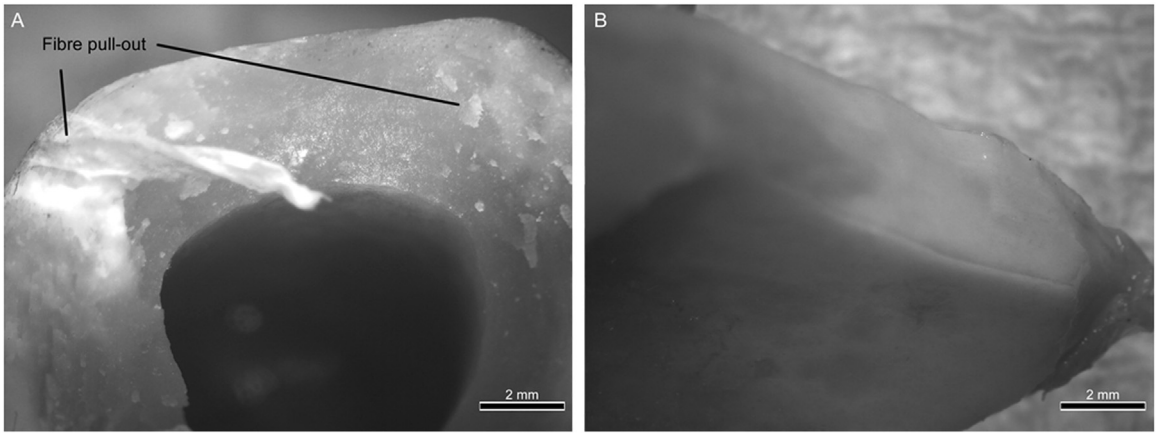

Fig. 5. (A) Fractured surface from a transverse fracture that resulted from testing at a slow strain rate (BS1) shows signs of fibre pull-out. (B) Fracture from a bone tested at high strain rate has a smoother surface (BM2) compared to (A). The images were taken with a Leica EZ 4D stereo microscope.

resistance is higher in the transverse direction than in the longitudinal direction, which is parallel to the orientation of the osteons and cement lines (Nalla et al., 2005). This allows bone to exhibit crack deflection as a toughening mechanism, since the longitudinal direction is the preferred path of fracture as it offers the least resistance (Koester et al., 2008). The fracture morphology that results is thus an outcome of a competition of the mechanical driving force, the path of least resistance, and bone toughening mechanisms (Launey et al., 2010). The effect of the bone toughening mechanism during fracture is to produce a highly tortuous crack surface that is not smooth, accompanied by a high energy to fracture (Currey and Butler, 1975; Nalla et al., 2005). The greater plastic deformation prior to failure and higher energy to fracture as seen in spiral fractures at lower strain rates point to the presence of strain toughening mechanisms. In an idealised case, spiral fractures caused by direct stress would occur at 45° and the fracture angle of 41.5° at higher strain rate suggests the dominance of principal strain. These two reasons could explain why secondary longitudinal fractures occurred at lower strain rates in torsional testing, and the spiral fractures produced at lower strain rates have a smaller angle to the long axis (Figs. 6 and 7). However, the consistent generation of spiral fractures shows that ovine tibiae fail primarily in their principal directions due to normal stress, regardless of strain rate, and indicates that the mechanical driving force plays the dominant effect here (Fig. 8).

4.2. Four-point bending tests

It is difficult to compare the results obtained in four-point bending to existing literature data as there is no four-point bending work of ovine bones to failure published in the open literature. The values obtained in this study are similar to the data presented by Ebacher et al. (2007) who fractured whole adult human tibiae of age 67 to 88 years, at a speed of 6 mm/min (0.0003 s^{-1}) in four-point bending, and reported a maximum load of 4.25 kN at a strain of 1.2%. Similar to the case of torsional stiffness, the bending stiffness of lamb tibiae is very close to the result reported for adult human tibiae at 2 kN/mm even though the latter were loaded at a much lower speed of 0.05 mm/s. The bending stiffness of the bones was significantly lower at the lower strain rate of 0.003–0.004 s^{-1} than at the higher strain rates of 0.08–0.1 s^{-1}. This effect agrees well with the viscoelastic data in bending presented by Buechner et al. (2001). On the other hand, strain-rate dependency is not expected in torsional loading as the strain rate would need to differ by four orders of magnitude before the normalised shear modulus decreases by 0.2 (Lakes et al., 1979).

Transverse fracture patterns have been observed in both three-point and four-point bending tests at quasi-static strain rates (Ebacher et al., 2007; Pierce et al., 2000). However, a plethora of fracture patterns have been reported in dynamic three-point bending tests where the testing speed was greater than 1.5 m/s (Forman et al., 2012; Kress et al., 1995). The work in this study bridged the gap by covering para-physiological strain rates (Juszczyk et al., 2011) at 0.08–0.3 s^{-1} on top of quasi-static strain rate at 0.003–0.004 s^{-1}. The consistent generation of a transverse fracture agrees well with the three-point bending results of immature pig femurs (Pierce et al., 2000). However, the four-point bending work of whole and machined adult human tibiae (Ebacher et al., 2007; Mercer et al., 2006) at quasi-static strain rates reported cases of cracks that initiated transversely on the tension side of the bone, but that fail obliquely on the compressive side, in shear. The fractures in this study also displayed two different failure modes, but longitudinal cracks were seen across strain rates (Figs. 3 and 4). This difference could be reconciled by the fact that both oblique and longitudinal fractures form in shear. However, this study differed from the earlier work by the use of a rocker mechanism at the cross-head of the testing machine, to introduce an extra degree of freedom

Table 2
Summary of the results of the torsional loading tests shows a spread of fracture torque but similar torsional stiffness.

Specimen	Peak torque (Nm)	Fracture torque (Nm)	Torsional stiffness (Nm/deg)	Energy to fracture (J)	Fracture pattern	Fracture location
TF1	45.64	44.86	2.61	482.07	Spiral	Proximal
TF2	23.49	23.44	1.56	177.01	Spiral	Proximal
TF3	26.92	26.37	1.49	266.30	Spiral	Proximal
TF4	60.14	60.14	2.73	740.01	Spiral - multiple	Proximal
Mean (SD)	39.05 (17.10)	38.70 (17.15)	2.10 (0.66)	416.35 (250.91) *	–	–
TS1	57.71	57.71	2.28	873.44	Spiral	Middle
TS2	57.76	57.69	2.70	753.83	Spiral - longitudinal	Middle
TS3	41.06	41.04	1.82	490.71	Spiral	Middle
TS4	65.42	64.60	3.35	1321.89	Spiral - multiple	Middle
Mean (SD)	55.48 (10.28)	55.26 (10.02)	2.54 (0.65)	859.97 (346.97) *	–	–

There was a significant increase in the work energy to fracture for the slower group. TF= fast group, TS= slow group.

Fig. 6. (Top) The progression of a 'clean' spiral fracture that took place over 0.572 ms in three video frames (frame rate of 7000 fps) for a tibia tested at the low strain rate (specimen TS4). The fracture angle occurred at approximately 30°. (Bottom) The progression of spiral fractures with several fracture paths of about 45° (specimen TF4) acquired at 10,000 fps.

that enabled the bone to self-align. This ensured that the bone was always in contact with the rollers and it eliminated other eccentric loading from being applied to the bone. Since the preferred path of fracture is along the lines of weakness of the cement lines in the longitudinal direction (Koester et al., 2008), a longitudinal crack is the simplest form of shear fracture. Initially, the mechanical driving force overpowers the toughening mechanisms. However, as the strain energy gets used up in the formation of transverse fracture, the effect of bone toughening mechanisms becomes more dominant, causing crack formation to slow down and produce a longitudinal crack that has signs of fibre pull-out (Fig. 5). This is similar to rough fracture surface demonstrated by Currey and Butler (1975) when bones were tested at slow strain rates. It is the formation of such a tortuous fracture path, and the minimal amount of strain energy applied to the bone at lower strain rate, that results in the greenstick (incomplete) fractures (Currey and Butler, 1975) that were seen in some of the specimens in this study.

Fragmented and comminuted fractures are viewed clinically as the result of a large impact on the bone and the results from Kress et al. (1995) support this clinical reasoning. The tibiae tested at para-physiological strain rates of 0.08–0.3 s^{-1} exhibited only 3 out of the 9 fracture patterns detailed in Kress et al. (1995). Indeed, in their study, transverse fractures only occurred in 4 out of 50 specimens when impacted at a speed of 7.5 m/s and 3 out of 11 specimens when tested at 1.2 m/s. It is worth pointing out that only 3 fracture patterns (oblique, tension wedge and transverse fractures) were observed at the lower testing rate of 1.2 m/s. At higher strain rates, comminuted fractures occur as the material fails at multiple locations, due to the development of stress concentration that exceeds the material endurance limit (Hibbeler, 2008). In our tests at higher strain rates, transverse fractures initiated within the inner span while oblique fractures initiated on the proximal side of the bone, between the inner and outer span. As the proximal end of the bone is wider than the distal end, potentially a larger bending moment would be required to initiate

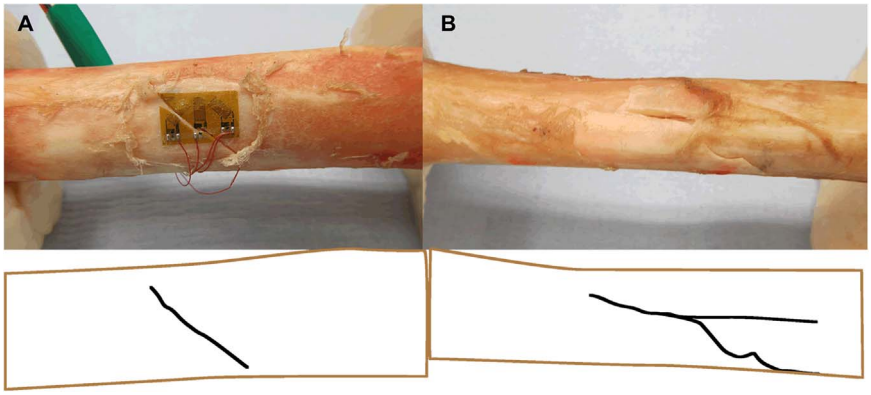

Fig. 7. Posterior views of two different types of spiral fractures with the line tracings below the photos. (A) A 'clean' spiral fracture that broke through the strain gauge, produced at the higher strain rate (specimen TF2) at about 45°. (B) Secondary longitudinal fracture was produced in this case after the initiation of the spiral fracture (about 30°) at the lower strain rate (specimen TS2).

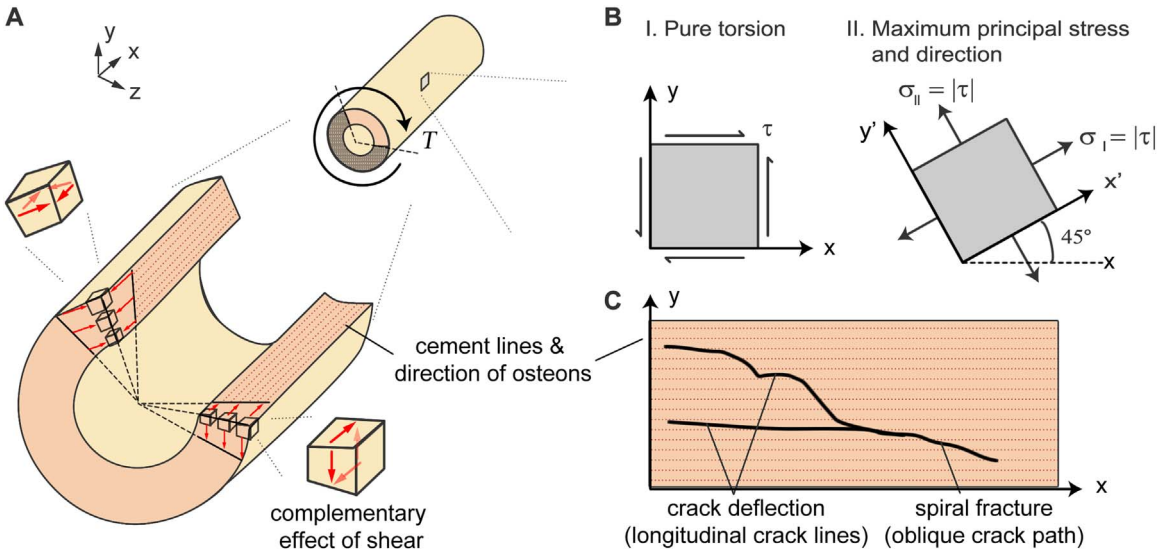

Fig. 8. (A) The application of a torque (T) causes bone to experience shear stress (and strain) in both the transverse and axial planes due to the complementary nature of shear. The maximum shear stress (τ) always occurs at a distance furthest from the centroid. (B) The state of stress at torsion means that the maximum principal stress (σ_1) occurs at 45° in tension, according to the principle of stress transformation. (C) The crack initiation is driven by the external torque, leading to a spiral fracture. As the energy gets used up, bone toughening mechanisms becomes more dominant, and cause crack deflection and longitudinal fracture to occur. [This fracture pattern is taken from specimen TS2 (Fig. 7B).].

the fracture, which could have contributed to the higher stiffness observed in oblique fractures than transverse fractures. However, there is also a possibility that oblique fractures may have occurred under three-point loading rather than four-point loading, due to the possibility that the equipment was unable to correct for misalignment of bones at high strain rates. The initiation of a fracture on the proximal side of the bone where there is a larger moment of inertia would suggest the storage of higher strain energy than a bone that broke distally with a transverse fracture. This could explain why there was more comminution associated with oblique fractures and a larger work to fracture than transverse fractures. This larger variance observed would have contributed to the result that there were no statistical differences in the energy absorbed as a function of the strain rate.

Therefore, the results from this study show that, in the immature ovine specimens, there was a differentiation of fracture patterns and bending stiffness at different strain rates in four-point bending. In torsional loading, the strain rate dependency was exhibited by the lower work to fracture, presence of multiple fractures, and change in fracture obliquity at higher strain rates. This suggests a link between the velocity and energy of the injury, and the fracture pattern that is revealed in radiological images. Transverse fractures may reflect relatively low-energy events, while oblique and comminuted fractures may suggest higher impact energy. These tendencies may inform the evaluation of the case history given of a child who has sustained an injury.

4.3. Limitations

The tests conducted covered only a limited range of strain rates that were chosen based on loading speed as reported in case histories. Since whole bone testing of immature bones to failure at different strain rates has not been conducted before, this study could be improved if a larger range of strain rates were chosen. However, this was not done due to experimental limitations of the testing apparatus. Ovine bones exhibit both plexiform and osteonal structure, thus care must be taken in extending the results to immature human bones, especially as human bones are more heterogenous than animal bones in terms of material properties. The consistency of the results obtained in this study is partly due to the subject-specific alignment method used to ensure that the bones are tested along their principal directions that minimises the presence of eccentric loading, and fulfil a minimum width-to-span of 1:4. Such results may not be obtained for other bone types that do not have a predominant longitudinal direction, or are excessively curved, as they would not fulfil the minimum criterion. In addition, should the bones be tested along other directions in bending, rotation of the bones is expected to happen and consistent fractures may not be obtained. The results obtained in this study may not be repeatable if conducted under other experimental conditions, especially if the bones were not kept moist as their mechanical behaviour would change. A greater number of specimens would increase statistical confidence in the results. Moreover, only one breed of sheep was considered and the results may vary between breeds. Further testing under various different conditions, with increased number of specimens for each case, would be required to produce different types of fracture patterns that can be used to differentiate between accidental and non-accidental injuries. It would be useful to obtain similar data from other bones and species in the absence of human specimens.

Digital Imaging correlation (DIC) could be used to provide richer information by providing a strain map of the entire bone. Moreover, it would augment the use of high speed camera to ascertain the conditions of testing, including the identification of the presence of eccentric loading or incident 3-point bending modes. Future work should include testing at combined loading to better represent the case histories reported.

Acknowledgements

The four-point bending rig was manufactured with the assistance of Satpal S Sangha and Paolo Lo Giudice. The authors also gratefully acknowledge the support provided by the Natural History Museum, where the micro-CT scans were conducted. Vee San Cheong held the SIM-You Poh Seng Scholarship and the Department of Bioengineering studentship at Imperial College London. Angelo Karunaratne was supported by the Royal British Legion as part of the Centre for Blast Injury Studies. The Instron materials testing machine was provided by a grant from Arthritis Research UK.

References

Athanasiou, K., Zhu, C.-F., Lanctot, D., Agrawal, C., Wang, X., 2000. Fundamentals of biomechanics in tissue engineering of bone. Tissue Eng. 6 (4), 361–381.
Baumer, T.G., Powell, B.J., Fenton, T.W., Haut, R.C., 2009. Age dependent mechanical properties of the infant porcine parietal bone and a correlation to the human. J.

Biomech. Eng. 131 (11), 111006.
Buechner, P.M., Lakes, R.S., Swan, C., Brand, R.A., 2001. A broadband viscoelastic spectroscopic study of bovine bone: implications for fluid flow. Ann. Biomed. Eng. 29 (8), 719–728.
Caffey, J., 1946. Multiple fractures in the long bones of infants suffering from chronic subdural hematoma. *Radiology* 195, 163–173.
Carty, H.M.L., 1993. Fractures caused by child abuse. *J. Bone Jt. Surg.* 75-B, 849–857.
Cheong, V.S., Bull, A.M.J., 2015. A novel specimen-specific methodology to optimise the alignment of long bones for experimental testing. J. Biomech. 48 (16), 4317–4321.
Cristofolini, L., Conti, G., Juszczyk, M., Cremonini, S., Sint Jan, S.V., Viceconti, M., 2010. Structural behaviour and strain distribution of the long bones of the human lower limbs. J. Biomech. 43 (5), 826–835.
Cristofolini, L., Viceconti, M., 2000. Mechanical validation of whole bone composite tibia models. J. Biomech. 33, 279–288.
Currey, J., Butler, G., 1975. The mechanical properties of bone tissue in children. J. Bone Jt. Surg. 57 (6), 810–814.
Ebacher, V., Tang, C., McKay, H., Oxland, T.R., Guy, P., Wang, R., 2007. Strain redistribution and cracking behavior of human bone during bending. Bone 40 (5), 1265–1275.
Finlay, J., Hurtig, M., Hardie, W., Liggins, A., Batte, S., 1995. Geometrical properties of the ovine tibia: a suitable animal model to study the pin-bone interface in fracture fixation? Proc. Inst. Mech. Eng. H: J. Eng. Med. 209 (1), 37–50.
Forman, J. L., de Dios, E., Symeonidis, I., Duart, J., Kerrigan, J. R., Salzar, R. S., Balasubramanian, S., Segui-Gomez, M., & Kent, R. W. (2012). *Fracture tolerance related to skeletal development and aging throughout life: 3-point bending of human femurs*. Paper presented at the IRCOBI Conference Proceedings, Dublin, Ireland.
Haney, S.B., Boos, S.C., Kutz, T.J., Starling, S.P., 2009. Transverse fracture of the distal femoral metadiaphysis: a plausible accidental mechanism. Pediatr. Emerg. Care 25 (12), 841–844.
Hardy, S., Pipelzadeh, M., 1991. Static analysis of short beams. J. Strain Anal. Eng. Des. 26 (1), 15–29.
Hibbeler, R.C., 2008. Mechanics of Materials. Prentice Hall.
Hobbs, C.J., 1989. ABC of child abuse. Fract. BMJ 298 (6679), 1015–1018.
Jayakumar, P., Barry, M., Ramachandran, M., 2010. Orthopaedic aspects of paediatric non-accidental injury. J. Bone Jt. Surg. Br. 92-B (2), 189–195.
Juszczyk, M.M., Cristofolini, L., Viceconti, M., 2011. The human proximal femur behaves linearly elastic up to failure under physiological loading conditions. J. Biomech. 44 (12), 2259–2266.
Koester, K.J., Ager, J.W., Ritchie, R.O., 2008. The true toughness of human cortical bone measured with realistically short cracks. Nat. Mater. 7 (8), 672–677.
Kowal-Vern, A., Paxton, T.P., Ros, S.P., Lietz, H., Fitzgerald, M., Gamelli, R.L., 1992. Fractures in the Under 3-Year-Old Age Cohort. Clin. Pediatr. *31*, 653–659.
Kress, T. A., Porta, D. J., Snider, J. N., Fuller, P. M., Psihogios, J. P., Heck, W. L., Frick, S. J., & Wasserman, J. F. (1995). *Fracture patterns of human cadaver long bones*. Paper presented at the International Research of Crash Biomechanics and Impact (IRCOBI), Brunnen, Switzerland.
Lakes, R.S., Katz, J.L., Sternstein, S.S., 1979. Viscoelastic properties of wet cortical bone—I. Torsional and biaxial studies. J. Biomech. 12 (9), 657–678.
Launey, M.E., Buehler, M.J., Ritchie, R.O., 2010. On the mechanistic origins of toughness in bone. Annu. Rev. Mater. Res. 40 (1), 25–53.
Leventhal, J.M., 1999. The challenges of recognizing child abuse: seeing is believing. J. Am. Med. Assoc. 281 (7), 657–659.
Mercer, C., He, M.Y., Wang, R., Evans, A.G., 2006. Mechanisms governing the inelastic deformation of cortical bone and application to trabecular bone. Acta Biomater. 2 (1), 59–68.
Miltner, E., Kallieris, D., 1989. Quasistatische und dynamische Biegebelastung des kindlichen Oberschenkels zur Erzeugung einer Femurfraktur. Z. für Rechtsmed. 102 (8), 535–544.
Moreno, J., Forriol, F., 2002. Effects of preservation on the mechanical strength and chemical composition of cortical bone: an experimental study in sheep femora. Biomaterials 23 (12), 2615–2619.
Nafei, A., Danielsen, C.C., Linde, F., I., Hvid, 2000. Properties of the growing trabecular ovine bone. Part 1: Mechanical and physical properties. *J. Bone Jt. Surg*. 82-B, 910–920.
Nalla, R.K., Stölken, J.S., Kinney, J.H., Ritchie, R.O., 2005. Fracture in human cortical bone: local fracture criteria and toughening mechanisms. J. Biomech. 38 (7), 1517–1525.
Osterhoff, G., Löffler, S., Steinke, H., Feja, C., Josten, C., Hepp, P., 2011. Comparative anatomical measurements of osseous structures in the ovine and human knee. Knee 18 (2), 98–103.
Ouyang, J., Zhu, Q., Zhao, W., Xu, Y., Chen, W., Zhong, S., 2003. Biomechanical character of extremity long bones in children. Chin. J. Clin. Anal. 21 (6), 620–623.
Pierce, M.C., Bertocci, G.E., 2008. Injury biomechanics and child abuse. Annu. Rev. Biomed. Eng. 10, 85–106.
Pierce, M.C., Bertocci, G.E., Vogeley, E., Moreland, M.S., 2004. Evaluating long bone fractures in children: a biomechanical approach with illustrative cases. Child Abus. Negl. 28 (5), 505–524.
Pierce, M.C., Valdevit, A., Anderson, L., Inoue, N., Hauser, D.L., 2000. Biomechanical evaluation of dual-energy X-ray absorptiometry for predicting fracture loads of the infant femur for injury investigation: an in vitro porcine model. J. Orthop. Trauma 14 (8), 571–576.
Stotts, A.K., 2007. Orthopaedic aspects of child abuse. Curr. Opin. Orthop. 18 (6), 550–554, [510.1097/BCO.1090b1013e3282ef1096ecc].
Taylor, D., O'Reilly, P., Vallet, L., Lee, T.C., 2003. The fatigue strength of compact bone in torsion. J. Biomech. 36 (8), 1103–1109.
Varghese, B., Short, D., Penmetsa, R., Goswami, T., Hangartner, T., 2011. Computed-tomography-based finite-element models of long bones can accurately capture strain response to bending and torsion. J. Biomech. 44 (7), 1374–1379.
Wullschleger, M., 2010. Effect of Surgical Approach on Bone Vascularisation, Fracture and Soft Tissue Healing: Comparison of Less Invasive to Open Approach, PhD. Queensland University of Technology, Brisbane.